INL/CON-06-12033
PREPRINT

Development of GAMMA Code and Evaluation for a Very High Temperature Gas-Cooled Reactor

ANS Meeting

C. Oh
H. C. No
H. S. Lim
E. S. Kim
J. H. Kim

June 2007

The INL is a
U.S. Department of Energy
National Laboratory
operated by
Battelle Energy Alliance

Development of GAMMA Code and Evaluation for a Very High Temperature Gas-Cooled Reactor

C. Oh*[1], H.C. NO[2], H.S. Lim[3], E.S. Kim[1], J.H. Kim[2]

P.O. Box 1625
[1]*Idaho National Laboratory, Idaho Falls, ID. 83415-3885, USA*
Email: chang.Oh@inl.gov, Phone: 208-526-7716, Fax: 208-526-0528

[2]*Korea Advanced Institute of Science and Technology*
373-1 Guseong-dong, Yuseong-gu, Teajon, Korea 305-701

[3]*Korea Atomic Energy Research Institute*
373-1 Dukjin-dong, Yuseong-gu, Taejon, Korea 305-353

Abstract - The very high-temperature gas-cooled reactor (VHTR) is envisioned as a single- or dual-purpose reactor for electricity and hydrogen generation. The concept has average coolant temperatures above 900^0C and operational fuel temperatures above 1250^0C. The concept provides the potential for increased energy conversion efficiency and for high-temperature process heat application in addition to power generation. While all the High Temperature Gas Cooled Reactor (HTGR) concepts have sufficiently high temperature to support process heat applications, such as coal gasification, desalination or cogenerative processes, the VHTR's higher temperatures allow broader applications, including thermochemical hydrogen production. However, the very high temperatures of this reactor concept can be detrimental to safety if a loss-of-coolant accident (LOCA) occurs. Following the loss of coolant through the break and coolant depressurization, air will enter the core through the break by molecular diffusion and ultimately by natural convection, leading to oxidation of the in-core graphite structure and fuel. The oxidation will accelerate heatup of the reactor core and the release of toxic gasses (CO and CO2) and fission products. Thus, without any effective countermeasures, a pipe break may lead to significant fuel damage and fission product release. Prior to the start of this Korean/United States collaboration, no computer codes were available that had been sufficiently developed and validated to reliably simulate a LOCA in the VHTR. Therefore, we have worked for the past three years on developing and validating advanced computational methods for simulating LOCAs in a VHTR.

This paper describes the governing equations and numerical methods used in GAMMA code and presents a portion of verification along with turbomachinery models that are being developed and linked to GAMMA code

I. INTRODUCTION

The VHTR reference concepts are helium-cooled, graphite-moderated, thermal neutron spectrum reactors with an outlet temperature while initially set up to 1000^0C. The high temperature will allow the reactor to be used for a large number of process heat applications, including hydrogen production.

The VHTR reactor core could be either a prismatic graphite block type core or a pebble bed core. Use of various working coolants is also being evaluated. [1] The process heat for hydrogen production will be transferred to the hydrogen plant through an intermediate heat exchanger (IHX). The reactor thermal power and core configuration will be designed to assure passive decay heat removal without fuel damage during hypothetical accidents. The fuel cycle will be a once-through very high burnup low-enriched uranium fuel cycle.

The basic technology for the VHTR [2] has been established in the former high-temperature gas-cooled reactor test and demonstration plants (DRAGON, Peach Bottom, AVR, Fort St. Vrain, and THTR). In addition, the technologies for the VHTR are being advanced in the Gas Turbine-Modular Helium Reactor (GT-MHR) Project [3], and the South African state utility ESKOM sponsored project to develop the Pebble Bed Modular Reactor (PBMR) [4]. Furthermore, the Japanese HTTR and Chinese HTR-10 test reactors are demonstrating the feasibility of some of the planned VHTR components and materials. (The HTTR reached a maximum coolant outlet temperature of 950^0C in 2004.) Therefore, the VHTR project is focused on building a demonstration reactor, rather than simply confirming the basic feasibility of the concept.

One or more technologies will use heat from the high-temperature helium coolant to produce hydrogen. The first technology of interest is the thermochemical splitting

of water into hydrogen and oxygen. There are a large number of thermochemical processes that can produce hydrogen from water, the most promising of which are sulfur-based and include the sulfur-iodine, hybrid sulfur-electrolysis, and sulfur-bromine processes (which operate in the 750 to 1000^0 C range). The second technology of interest is thermally assisted electrolysis of water. The high-efficiency Brayton cycle enabled by the VHTR may be used to generate the hydrogen from water by electrolysis. The efficiency of this process can be substantially improved by heating the water to high-temperature steam before applying electrolysis.

II. GOVERNING EQUATIONS

analysis for VHTR as part of ROK/US I-NERI project GAMMA code was developed specifically for air ingress [5]. The governing equations and numerical methods adopted for this project are described below.

The multi-dimensional governing equations for a chemically reacting flow [6] consist of the basic equations for continuity, momentum conservation, energy conservation of the gas mixture, and the mass conservation of each species. Six gas species (He, N_2, O_2, CO, CO_2, and H_2O, (NO, 2004)) are considered in the present analytical model, and it is assumed that each gas species and the gas mixture follow the equation of state for an ideal gas. The GAMMA code has the capability to handle the thermo-fluid and chemical reaction behaviors in a multi-component mixture system as well as heat transfer within the solid components, free and forced convection between a solid and a fluid, and radiative heat transfer between the solid surfaces. Also, the basic equations are formulated with a porous media model [7] to consider heat transport in a pebble-bed core) as well as solid-fluid mixed components.

The equation of continuity for the gas mixture:

$$\varphi\frac{\partial\rho}{\partial t}+\nabla\cdot\left(\rho\mathbf{u}\right)=\varphi\sum_s R_s \tag{2-1}$$

The equation of momentum conservation:

$$\rho\left(\frac{1}{\varphi}\frac{\partial\mathbf{u}}{\partial t}+\frac{1}{\varphi^2}\mathbf{u}\cdot\nabla\mathbf{u}\right)=-\nabla P+\frac{1}{\varphi}\nabla\cdot\left(\mu\bar{N}\mathbf{u}\right)-\frac{\mu}{K}\mathbf{u}-\frac{C_F\rho}{\sqrt{K}}|\mathbf{u}|\mathbf{u}+\rho\mathbf{g} \tag{2-2}$$

The equation of sensible energy conservation:

$$\varphi\frac{\partial}{\partial t}(\rho H)+\nabla\cdot(\rho\mathbf{u}H)=\nabla\cdot\left[\left(\varphi\lambda_f+\lambda_{disp}\right)\nabla T_f\right]-\nabla\cdot\left(\varphi\sum_{s=1}^{m}H_s\mathbf{J}_s\right)-\varphi\sum_s\Delta h_{f_s}^o R_s+h_{sf}a_{sf}\left(T_p-T_f\right) \tag{2-3}$$

The conservation equation of each species, s:

$$\varphi\frac{\partial}{\partial t}(\rho Y_s)+\nabla\cdot(\rho\mathbf{u}Y_s)=-\nabla\cdot(\varphi\mathbf{J}_s)+\varphi R_s \tag{2-4}$$

and for He, $Y_m=1-\sum_{s=1}^{m-1}Y_s$

The equation of state for an ideal gas:

$$\rho=\frac{P}{\bar{R}T}\left(\sum_{s=1}^{m}Y_s/W_s\right)^{-1} \tag{2-5}$$

For a solid and a pebble bed, the same heat conduction equation is used. A thermal non-equilibrium model for porous media is used to consider the heat exchange between the fluid and the pebbles as follows:

$$\left[(1-\varphi)(\rho C)_p\right]\frac{\partial T_p}{\partial t}=\nabla\cdot\left(\lambda_{eff}\nabla T_p\right)+q'''-h_{sf}a_{sf}\left(T_p-T_f\right) \tag{2-6}$$

Radiative heat transfer in the enclosure is well-modeled by using an irradiation/radiosity method [8] which assumes that the fluid is non-participating and the radiation exchange between surfaces is gray and diffuse. The net radiative flux from agglomerated surface k, which consists of N_k faces of the original mesh, is given by

$$q_{rk}''=\left[\left(\sum_{j\neq k}^{M}F_{kj}\right)\varepsilon_k\bar{T}_k^4-\varepsilon_k\sum_{j\neq k}^{M}F_{kj}J_j\right]\left[\varepsilon_k+(1-\varepsilon_k)\sum_{j\neq k}^{M}F_{kj}\right]^{-1}$$
$$J_j=\varepsilon_jC_j\sigma\bar{T}_j^4+(1-\varepsilon_j)C_j\sum_{i\neq j}^{M}F_{ji}J_i \tag{2-7}$$

The ordinary diffusion flux (J_s) is given in two forms, the full multi-component diffusion [9] and the effective diffusion [10] by the assumption that a dilute species, s, diffuses through a homogeneous mixture:

$$\mathbf{J}_s=\rho\frac{W_s}{W^2}\sum_{k=1,k\neq s}^{m}\left[D_{sk}\nabla\left(Y_kW\right)\right] \tag{2-8}$$

$$\mathbf{J}_s=-\rho D_{s-mix}\nabla Y_s \quad where \quad D_{s-mix}=\left(\sum_{k=1,k\neq s}^{m}X_k/\mathbf{D}_{sk}\right)^{-1} \quad (\mathrm{m}\geq 3) \tag{2-9}$$

Although Eq. (2-8) predicts the accurate diffusion behaviors of species in a multi-component mixture, Eq. (2-9) is generally used in numerical calculation because of its computational efficiency and its accuracy close to that of Eq. (2-8). Physical properties, such as molar weight, viscosity, thermal conductivity, and sensible enthalpy, for each gas component and gas mixtures, are obtained from the handbooks of gas properties [11-12].

III. NUMERICAL METHOD

The governing equations are discretized in a semi-implicit manner in the staggered mesh layout and then dependent variables are linearized by the Newton method. For a fast computation, the Implicit Continuous Eulerian (ICE) technique [13] is adopted to reduce a 10N×10N whole system matrix to a N×N pressure difference matrix.

All the conservation equations, Eqs. (2-1) - (2-4), are discretized as follows:

$$\varphi_i \frac{\rho_i^{n+1}-\rho_i^n}{\Delta t}+\nabla_i\cdot\left(\dot{\rho}^n\mathbf{u}^{n+1}\right)=\varphi_i\sum_s R_{s\,i}^{\,n+1}, \tag{3-1}$$

$$\begin{aligned}\frac{1}{\varphi_j}\frac{\mathbf{u}_j^{n+1}-\mathbf{u}_j^n}{\Delta t}+\frac{1}{\varphi_j^2}\mathbf{u}_j^n\cdot\nabla_j\left(\mathbf{u}^n\right)&=-\frac{1}{\bar{\rho}_j^{\,n}}\nabla_j\left(P^{n+1}\right)+\frac{1}{\bar{\rho}_j^{\,n}\varphi_j}\nabla_j\left[\mu^n\nabla\left(\mathbf{u}^n\right)\right]\\&-\frac{\bar{\mu}_j^{\,n}}{K_j}\mathbf{u}_j^{n+1}-\frac{C_{Fj}\bar{\rho}_j^{\,n}}{\sqrt{K_j}}\left|\mathbf{u}_j^{n+1}\right|\mathbf{u}_j^{n+1}+\mathbf{g}_j^n\end{aligned} \tag{3-2}$$

$$\begin{aligned}\varphi_i\frac{\left(\rho H\right)_i^{n+1}-\left(\rho H\right)_i^n}{\Delta t}+\nabla_i\cdot\left(\dot{\rho}^n\dot{H}^n\mathbf{u}^{n+1}\right)&=\nabla_i\cdot\left[\left(\varphi\lambda_f+\lambda_{disp}\right)^n\nabla\left(T_f^{\,n}\right)\right]\\&-\nabla_i\cdot\left[\sum_{s=1}^{m}\left(\varphi\bar{H}_s^{\,n}\mathbf{J}_s^{\,n}\right)\right]-\varphi_i\sum_s\Delta h_{f_s}^{o}R_{si}^{n+1}\\&+h_{sf_i}^{\,n}a_{sf}\left(T_p-T_f\right)_i^n\end{aligned} \tag{3-3}$$

$$\varphi_i\frac{\left(\rho Y_s\right)_i^{n+1}-\left(\rho Y_s\right)_i^n}{\Delta t}+\nabla_i\cdot\left(\dot{\rho}^n\dot{Y}_s^{\,n}\mathbf{u}^{n+1}\right)=-\nabla_i\cdot\left(\varphi\mathbf{J}_s^{\,n}\right)+\varphi_i R_{s\,i}^{\,n+1} \tag{3-4}$$

where a bar (-) indicates average property and a dot (·) indicates donor property (1st-order upwind) which depends on flow direction. In the staggered mesh, i is the index of a scalar cell and j is the index of a momentum cell.

Using the Newton method, pressure is linearized as $P^{n+1}\rightarrow P^k+\delta P$ and then inserted into Eq. (3-2), resulting in the following form:

$$\mathbf{u}_j^{\,n+1}=\mathbf{u}_j^{\,k}+\left(\frac{d\mathbf{u}}{dP}\right)_j\nabla_j\left(\delta P\right) \tag{3-5}$$

where $\left(\frac{d\mathbf{u}}{dP}\right)_j$ is the partial derivative of velocity component with respect to pressure. Other dependent variables and the source terms treated implicitly also are linearized as follows:

$$\begin{aligned}&Y_s^{n+1}\rightarrow Y_s^k+\delta Y_s,\quad T^{n+1}\rightarrow T^k+\delta T\\&\rho^{n+1}\rightarrow\rho^k+\left(\frac{\partial\rho}{\partial P}\right)^k\delta P+\left(\frac{\partial\rho}{\partial T}\right)^k\delta T+\sum_s\left(\frac{\partial\rho}{\partial Y_s}\right)^k\delta Y_s\\&H^{n+1}\rightarrow H^k+\left(\frac{\partial H}{\partial T}\right)^k\delta T+\sum_s\left(\frac{\partial H}{\partial Y_s}\right)^k\delta Y_s\\&R_s^{\,n+1}\rightarrow R_s^{\,k}+\sum_s\left(\frac{\partial R_s}{\partial Y_s}\right)^k\delta Y_s\end{aligned} \tag{3-6}$$

By inserting $\mathbf{u}_j^{\,n+1}$ of Eq. (3-5) and linearized variables (ρ_i^{n+1}, $Y_{si}^{\,n+1}$, $T_{f\,i}^{\,n+1}$, H_i^{n+1}, $R_{si}^{\,n+1}$) into the discretized scalar equations, Eqs. (3-1), (3-3), and (3-4), and then combining all the resulting equations together into a linear algebraic form, a 7×7 square matrix is obtained:

$$\underline{\underline{B}}\,\underline{\delta X}=\underline{b}+\underline{a}\,\delta P_C+\underline{c}\left(\delta P_E\right)+\underline{d}\left(\delta P_W\right)+\underline{e}\left(\delta P_T\right)+\underline{f}\left(\delta P_B\right)+\underline{g}\left(\delta P_N\right)+\underline{h}\left(\delta P_S\right)$$

where $\left[\delta\underline{X}\right]^T=\left[\delta P\ \delta T_f\ \delta Y_{N_2}\ \delta Y_{O_2}\ \delta Y_{CO}\ \delta Y_{CO_2}\ \delta Y_{H_2O}\right]^T$ (3-7)

Multiplying Eq. (3-7) by the inverse matrix of $\underline{\underline{B}}$, the solution vector is expressed as

$$\delta\underline{X}=\underline{b}'+\underline{a}'\,\delta P_C+\underline{c}'\left(\delta P_E\right)+\underline{d}'\left(\delta P_W\right)+\underline{e}'\left(\delta P_T\right)+\underline{f}'\left(\delta P_B\right)+\underline{g}'\left(\delta P_N\right)+\underline{h}'\left(\delta P_S\right) \tag{3-8}$$

As a result, the first row in Eq. (3-8) becomes the N×N pressure matrix. The remaining rows, the fluid temperature and the mass fraction of each species, are expressed as a function of pressure only. The above calculation process is repeated until the convergence criterion, $\varepsilon=\max\left(\delta P_i/P_i^k\right)$, is satisfied. According to whether the convergence succeeds or fails, the time step size is controlled but restricted by the maximum time step limit,

$\Delta t_{\max}\ \le\ \min\left(\Delta t_{convective},\,\Delta t_{viscous},\,\Delta t_{conductive},\,\Delta t_{diffusive}\right)$, due to explicit treatment of the second-order terms.

The heat conduction equation, Eq. (2-6), is solved by the Crank-Nicolson method and coupled with the thermo-fluid calculation explicitly or implicitly.

$$\begin{aligned}\left[\left(1-\varphi\right)\left(\rho_pC_p\right)_i^n\right]\frac{\left(T_p\right)_i^{n+1}-\left(T_p\right)_i^n}{\Delta t}&=q_{N_i}^{\prime\prime\,n}-h_{sf_i}^{\,n}\left(T_{p_i}^{\,n}-T_i^n\right)\\&+\frac{\theta}{Vol_i}\nabla_i\cdot\left(\bar{\lambda}_{eff}\nabla T_p^{\,n+1}\right)++\frac{1-\theta}{Vol_i}\nabla_i\cdot\left(\bar{\lambda}_{eff}\nabla T_p^{\,n}\right)\end{aligned} \tag{3-9}$$

$$a_cT_p^{\,c}+a_wT_p^{\,w}+a_eT_p^{\,e}+a_bT_p^{\,b}+a_tT_p^{\,t}+a_sT_p^{\,s}+a_nT_p^{\,n}=b_c \tag{3-10}$$

The above solution scheme is applicable to a 1-D piping flow network with simple structure re-arrangement. Therefore, a concerned system can be configured by the linkage of a 1-D calculation module and a 2/3-D calculation module

IV. VERIFICATION

Since at least five species must be considered in an air ingress accident and the concentrations of each species determine the chemical reaction rate as well as the buoyancy force driven by the density difference, it is essential to understand the diffusion behavior in the multi-component mixture system.

The apparatus of the "two bulbs" experiment [14] conducted by Duncan and Toor consisted of two bulbs and a small capillary tube. The bulbs had volumes of 77.99 cm^3 and 78.63 cm^3, respectively. The capillary tube joining them was 85.9 mm long and 2.08 mm in diameter. Initially the bulbs were isolated by a stopcock installed at the center of the capillary tube. The entire device was maintained at a temperature of 35.2°C in the atmospheric pressure. The initial concentrations of the

filling gases and the nodalization diagram for the simulation are given in Figure 1.

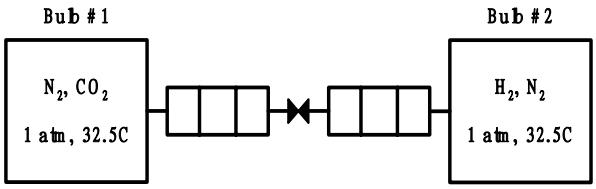

Bulb #1: $X_{H_2} = 0.$, $X_{N_2} = 0.50086$, $X_{CO_2} = 0.49914$

Bulb #2: $X_{H_2} = 0.50121$, $X_{N_2} = 0.49879$, $X_{CO_2} = 0.$

Figure 1. Initial conditions at each bulb.

As shown in Figure 2, the calculation results using the full multi-component diffusion form, Eq. (2-8), follow almost exactly the data measured at each bulb. Particularly, the exact prediction of N_2 gas behavior demonstrates the typical diffusion phenomena observed in the multi-component system: reverse diffusion in which a species moves against its own concentration gradient, osmotic diffusion in which a species diffuses even though its concentration gradient is zero and diffusion barrier when a species does not diffuse even though its concentration gradient is nonzero. More detailed validation and verification of GAMMA code can be found in [5].

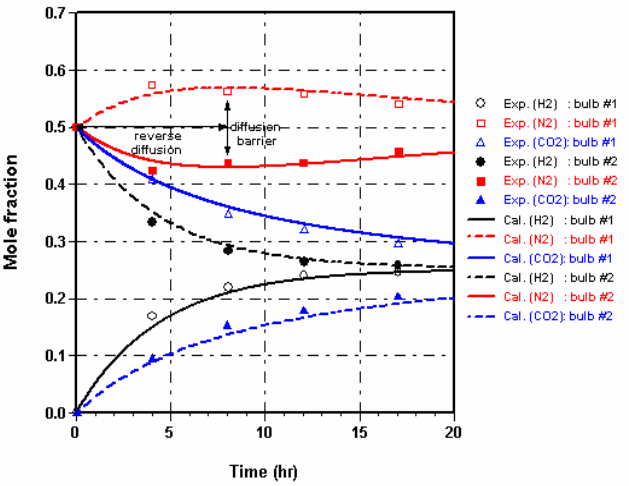

Figure 2. Calculation and Experimentation results for the mole fractions of each species for the "two bulbs experiment."

V. TURBO MACHINERY MODEL

We envision GAMMA code to be an integrated computer code for analyzing the HTGR coupled with hydrogen production plant . This means that we need to include the turbomachinery model and hydrogen production related model to GAMMA in the near future. Actually as part of this task, turbomachinery models are being developed [15] and are being linked to GAMMA code. The methodology of the model and some results are presented in this section.

The flow in multi-stage gas turbine is inherently three-dimensional. It is necessary to simplify the flow as having an intermediate level of sophistication, because the real flow process in a multistage gas turbine is exceedingly complex. The flow is assumed to be inviscid and may be regarded as being obtained by circumferentially averaging all flow properties, and then the loss effects are added on to the throughflow solution.

From the assumption of axisymmetric and inviscid flow it is possible to define a series of meridional stream surfaces and there are surfaces of revolution along which fluid particles are assumed to move through the gas turbine. In typical multi-stage axial compressor or turbine, the streamlines change radius along the axial length of the component, and the calculation of the flow along the hub to tip surface is usually referred to as the thoughflow method [16].

In the view of the meridional plane, Figure 3, the typical quasi-orthogonal lines and stream surface are illustrated. According to the description and approach given by [17], the acceleration of a fluid particle at P can be built up from the following components: $V_m \partial V_m / \partial m$ in the m direction, $-V_\theta^2 / r$ in the radial direction, and V_m^2 / r_c in the normal to the m direction. With the blade loading to be neglected, these three acceleration components can be combined to give the total acceleration a_q in the direction of the quasi-orthogonal line

$$a_q = V_m \frac{\partial V_m}{\partial m}\cos\alpha + \frac{V_m^2}{r_c}\sin\alpha - \frac{V_\theta^2}{r}\sin(\phi+\alpha) \qquad (5\text{-}1)$$

The momentum equation and energy equation applied in the stream surface is then

$$\frac{1}{2}\frac{d}{dq}V_m^2 = \frac{dh_0}{dq} - T\frac{ds}{dq} - \frac{1}{2r^2}\frac{d\left(r^2 V_\theta^2\right)}{dq} + \frac{V_m^2}{r_c}\sin\alpha + V_m\frac{dV_m}{dm}\cos\alpha \qquad (5\text{-}2)$$

and the total mass flow rate across the quasi-orthogonal is given by`

$$\dot{m} = \int_A^B 2\pi r \rho V_m \sin\alpha \; dq \qquad (5\text{-}3)$$

so that the meridional velocity and streamline curvature can be calculated from these two equations.

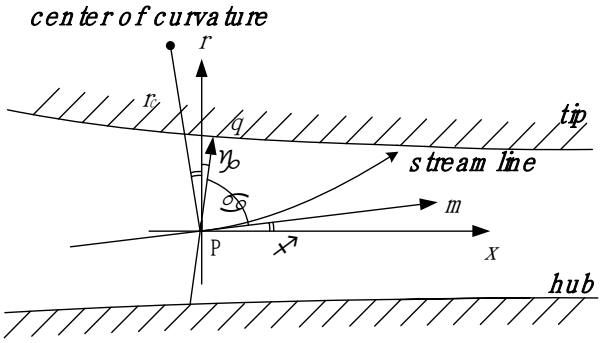

Figure 3.Quasi-orthogonal line in the meridional plane

The GTHTR300 compressor design of JAEA [18] has been selected to verify the code results. This particular unit has been chosen because the details of the compressor geometry and overall performance are available. Table 1 shows a summary of the design parameters. This compressor has a high reaction stage design and a constant inner wall diameter with high hub-tip ratio throughout 20 stages. In Table 2, the predictions by the present code are compared with the design-point performance of JAEA data. This table shows that the pressure and temperature conditions are well satisfied with the design-point loss estimation. The fluid properties and velocities in the compressor are calculated and the representative examples are shown in Figures 8 and 9. By modifying the loss models, this code is capable of estimating the performance of a wide range operation. The predicted pressure ratio results are compared with the reference data in Figure 10. The pressure ratio variation with the change of mass flow shows excellent agreement and the surge margin is also well predicted. While the reference shows 30% of surge margin, the code result is 30.9%. The JAEA data were replotted on the non-dimensional basis, polytropic efficiency against the corrected mass flow rate in Figure 11. The code result shows good agreement compared with the reference and the general trends of variation are well observed. The efficiency was slightly overestimated at low rotational speed with a RMS error about 3 percent.

Table 1. Specifications of GTHTR300 Compressor.

Mass flow rate (kg/s)	449.7
Inlet temperature (°C)	28
Inlet pressure (MPa)	3.52
Pressure ratio	2.0
Hub diameter (mm)	1500
Tip diameter (1st/20th stage, mm)	1704/1645
Number of stages	20
Rotational speed (rpm)	3600
Number of rotor/stator blades (1st stage)	72/94
Polytropic efficiency (%)	90.5

Table 2. Comparison of design-point performance.

Parameters	JAEA	KAIST	Error (%)
Pressure ratio	2.00	1.98	-1.00
Temperature ratio	1.36	1.35	-0.66
Polytropic efficiency(%)	90.5	90.7	0.22
Shaft Work (MW)	251	246	-1.99

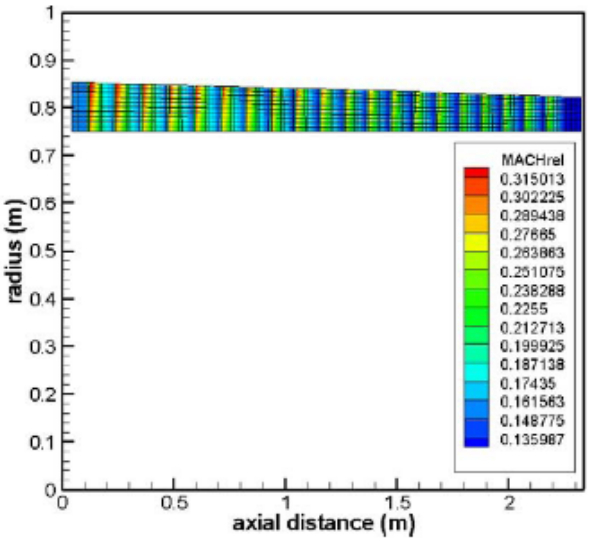

Figure 4. Relative Mach number in the compressor.

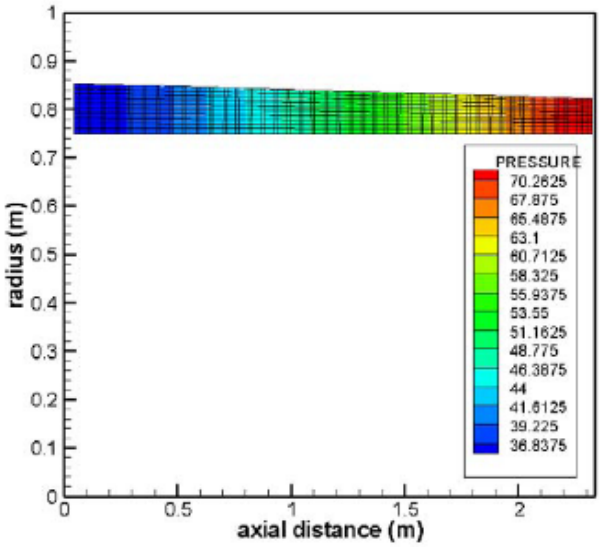

Figure 5. Total pressure in the compressor.

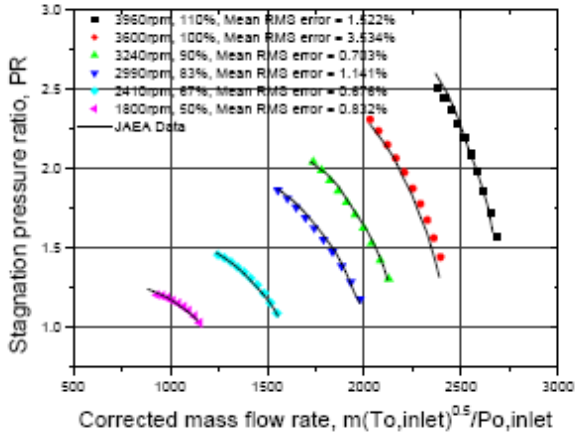

Figure 6. Pressure ratio vs. mass flow characteristics of GTHTR300 compressor.

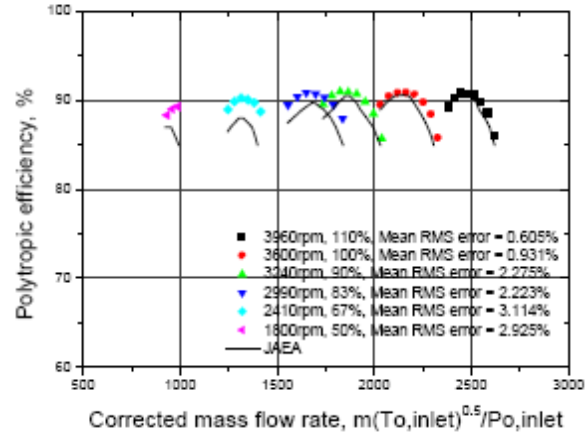

Figure 7. Efficiency vs. Mass flow characteristics of GTHTR300 compressor.

VI. COUPLING OF VHTR AND HTSE

The baseline plant configuration was based on Figure 8. In this configuration, an indirect cycle was used with the reactor coupled to the secondary side by means of an intermediate heat exchanger (IHX) as recommended by the Independent Technology Review Group [19]. The reactor was assumed to produce 600 MW of thermal power with a 900 °C outlet temperature with a nominal pressure of 7MPa and uses helium coolant on the primary side. The nominal rise in fluid temperature across the core was assumed to be 400 °C, based on the point design (MacDonald et al. 2003). The reactor pressure drop and the primary side pressure drop of the IHX are assumed to be 50 kPa.

The power conversion unit (PCU) [20] consists of a recuperated Brayton cycle. Referring to Figure 6, the fluid exits the IHX and the flow is split with most of the flow entering the PCU. The rest of the flow, approximately 10%, goes to the HTLHX. Upon entering the PCU the fluid enters the turbine for expansion. After leaving the turbine the fluid passes through the hot side of the recuperator and is further cooled by a precooler before entering the low pressure compressor. The fluid is cooled by an intercooler before entering the high pressure compressor. The fluid leaves the high pressure compressor and enters the cold side of the recuperator before combining with the fluid from the HTLHX and returning to the IHX.

The reactor was coupled to the hydrogen processing facility by means of an intermediate heat transport loop (IHTL). The IHTL was placed in parallel with the PCU as seen in Figure 8. It was assumed that 50 MW of thermal power are transported to the IHTL. A circulator is needed in the secondary side to account for pressure losses in the heat transport loop heat exchanger (HTLHX). Estimations of the required separation distance between the nuclear and hydrogen process plant vary considerably. For example, Sochet et al. [21] recommended 500 m for the High-Temperature Reactor while Smith et al. [22] recommended a separation distance of from 60 to 120 m for the VHTR and the hydrogen production plant. For this analysis, a nominal value of 90 m was used. The working fluid in the loop is assumed to be helium.

The coupling of the IHTL to the hydrogen processing facility was accomplished by means of three process heat exchangers (PHX). Figure 9 details the configuration of the 3 PHX's in the IHTL. Two heat exchangers in parallel are followed by one heat exchanger in series. This configuration was chosen to deliver high inlet temperatures on the hot side of the first two heat

exchangers where high cold side outlet temperatures are needed for the hydrogen production facility. The third heat exchanger however, does not require high cold side outlet temperatures and the hot side inlet temperature from the outlet of the prior heat exchangers is sufficient for heating the cold side fluid.

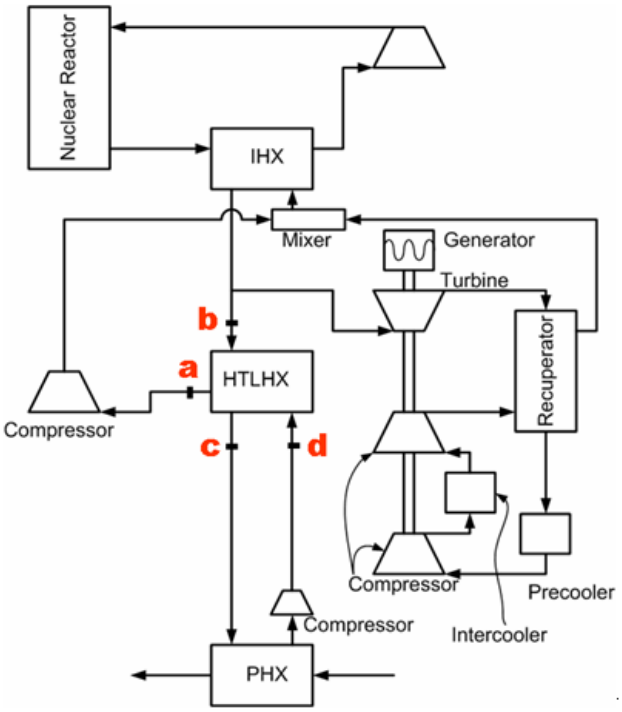

Figure 8. Baseline plant configuration for electrical and hydrogen production

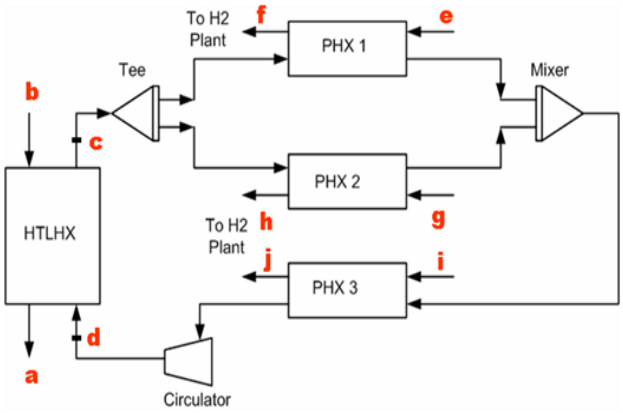

Figure 9. IHTL process heat exchanger configuration

The details of the HTSE is shown in Figure 10. The process water enters on the left. The water is then pumped up to the operating pressure of 5 MPa. The efficiency of the pumps and circulators is assumed to be 75%. This water is then combined with water condensate returned from the hydrogen/water product stream. This stream then enters the low temperature recuperator. The pressure drop through the heat exchangers is assumed to be 20 kPa. From there the steam is further heated by PHX 3. Upon leaving PHX 3 the steam is mixed with hydrogen from the product stream by a recirculator which works to overcome the pressure drops in the system. A mole fraction of 90% water and 10% hydrogen is maintained in this model. This hydrogen helps to maintain reducing conditions at the electrolysis stack to prevent oxidation. The mixed stream then enters the high temperature recuperator which takes advantage of the high temperature outlet from the electrolysis stack. The hydrogen/water stream is then heated to the operating temperature for the electrolysis stack, in this case 827 °C, in PHX 1.

The electrolyzer has another inlet stream that contains the sweep gas. This is used to sweep away the oxygen from the electrolysis process. A steam sweep gas is used in this model and enters the plant in the middle-bottom of Figure 8. It is first pumped up to operating pressure and then heated in a heat exchanger using the hot sweep outlet from the electrolyzer. Before it enters the electrolysis stack it is heated to the operating temperature of 827 °C in PHX 2.

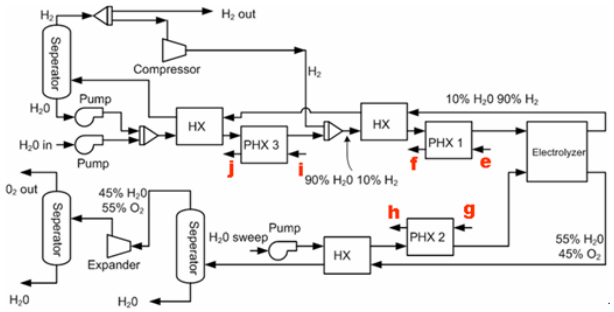

Figure 10. Schematic of HTSE process.

Upon leaving the electrolyzer, the product stream is 90% hydrogen and 10% water. This then passes through the high and low temperature recuperators. The steam condensate is then separated from the hydrogen and recycled back into the system. After leaving the electrolyzer, the sweep gas enters the recuperator to preheat the sweep inlet. The sweep outlet contains approximately 55% water and 45% oxygen. It is then partially separated before entering an expander to recuperate some of the power. The expander has an efficiency of 80%. Finally the sweep stream is further separated and high purity oxygen and water are produced.

In general, for an operating electrolysis stack, there will be a temperature change associated with the electrolysis

process. For these cases, the energy equation for electrolysis process can be written as [20]:

A. Energy Equation

An energy balance on the electrolyzer gives

$$\sum_i \dot{n}_{P-i}\, H_{P-i}(T_P, P) = \sum_i \dot{n}_{R-i}\, H_{R-i}(T_R, P) + Q + W \tag{6-1}$$

where $\dot{n}$ =species mole flow rate, H=enthalpy per mole, Q = rate of heat transfer to the electrolyzer, W = rate of electrical work supplied to the electrolyzer, T=temperature, P=pressure, and where we have used subscripts R for reactants and P for products. Their mass flowrates are defined

$$\begin{aligned} &m_{H_2O\text{-}o\text{-}cath}\, h_{H_2O}(T_o,P) + m_{H_2\text{-}o\text{-}cath}\, h_{H_2}(T_o,P) + m_{N_2\text{-}o\text{-}cath}\, h_{N_2}(T_o,P) \\ &\quad m_{O_2\text{-}o\text{-}anode}\, h_{O_2}(T_o,P) + m_{sweep\text{-}o\text{-}anode}\, h_{sweep}(T_o,P) = \\ &\qquad m_{H_2O\text{-}i\text{-}cath}\, h_{H_2O}(T_i,P) + m_{H_2\text{-}i\text{-}cath}\, h_{H_2}(T_i,P) + m_{N_2\text{-}i\text{-}cath}\, h_{N_2}(T_i,P) \\ &\qquad\quad m_{O_2\text{-}i\text{-}anode}\, h_{O_2}(T_i,P) + m_{sweep\text{-}i\text{-}anode}\, h_{sweep}(T_i,P) + Q + W \end{aligned} \tag{6-2}$$

where m = species mass flow rate (kg/s), h =specific enthalpy (joules/kg), and where subscripts i and o represent inlet and outlet, respectively.

B. Species Mole and Mass Flowrates

The species mole flowrates entering and leaving the electrolyzer are related to the current density through the relationships

$$\begin{aligned} \dot{n}_{H_2O-o-cath} &= \dot{n}_{H_2O-i-cath} - \frac{iA}{2F} \\ \dot{n}_{H_2-o-cath} &= \dot{n}_{H_2-i-cath} + \frac{iA}{2F} \\ \dot{n}_{O_2-o-anode} &= \dot{n}_{O_2-i-anode} + \frac{iA}{4F} \\ \dot{n}_{sweep-o-anode} &= \dot{n}_{sweep-i-anode} \\ \dot{n}_{N_2-o-cath} &= \dot{n}_{N_2-i-cath} \end{aligned} \tag{6-3}$$

where i= current density (amps/m^2), A=electrode surface area, (m^2) and F= Faradays constant.

The species mass flowrates and mole flowrates are related as follows: For an individual species

$$\dot{m}_{k-o} = A_k\, \dot{n}_{k-o} \text{ and } \dot{m}_{k-i} = A_k\, \dot{n}_{k-i}\ , \quad k = H_2O,\ H_2\ ,\ O_2, \text{ and } N_2. \tag{6-4}$$

where A_k is the atomic weight of species k in kg per mole and subscript o is the outlet and i is the inlet.

C. Cell Voltage and Electrical Work

The voltage drop across the electrolyzer is the sum of the electrode Nernst potential and the resistance of the cell. In estimating the resistance, the activation and the concentration overpotentials are lumped in with the cell internal resistance. The cell voltage is then assumed given by

$$V_{cell} = V_N + i \cdot r \tag{6-5}$$

where V_N= is the Nernst potential, and r = is the area-specific cell resistance (ohms-m^2).

The electrical work done in the cell is

$$W = V_{cell} \cdot i \cdot A\ . \tag{6-6}$$

The active species giving rise to the Nernst potential satisfy the chemical balance equation

$$H_2O\,(g) \rightarrow H_2\,(g) + \frac{1}{2} O_2\,(g)\cdot \tag{6-7}$$

The change in Gibbs free energy for this reaction carried out at temperature T and pressure P is

$$\Delta G(T,P) = \Delta G_f(T,P) + RT \ln\left[\frac{f_{H_2}\, f_{O_2}^{\frac{1}{2}}}{f_{H_2O}}\right] \tag{6-8}$$

where f is the molar fraction of a species and $\Delta G_f(T,P)$ is the Gibbs free energy in forming the products at temperature T and pressure P minus the same for the reactants, that is,

$$\Delta G_f(T,P) = G_{f-H_2}(T,P) + 1/2\, G_{f-O_2}(T,P) - G_{f-H_2O}(T,P)\ . \tag{6-9}$$

where $G_{f\text{-}i}(T,P)$ is the Gibbs free energy on a per mole basis of forming species i at conditions T and P. In turn $\Delta G_f(T,P)$ is written in terms of $\Delta G^0{}_f(T) = \Delta G_f(T, P_{STD})$ where P_{STD} = 0.101 MPa. Then setting the change in Gibbs free energy equal to the electrical work done the voltage developed by the cell is

$$V_{Nernst} = \frac{-1}{2F}\left[\Delta G_f{}^0(T) + RT \ln\left[\left(\frac{f_{H_2} f_{O_2}{}^{\frac{1}{2}}}{f_{H_2O}}\right)\left(\frac{P}{P_{STD}}\right)^{\frac{1}{2}}\right]\right] \quad (6\text{-}10)$$

where P_{STD} = 0.101 MPa and P is the cell pressure.

The mole fractions at any point in the electrolyzer are related to the molar mass flowrates at that point through

$$f_{H_2O-cath} = \frac{\dot{n}_{H_2O}}{\dot{n}_{H_2O} + \dot{n}_{H_2} + \dot{n}_{N_2}} \qquad f_{H_2-cath} = \frac{\dot{n}_{H_2}}{\dot{n}_{H_2O} + \dot{n}_{H_2} + \dot{n}_{N_2}}$$

$$f_{O_2-anode} = \frac{\dot{n}_{O_2}}{\dot{n}_{sweep} + \dot{n}_{O_2}} \qquad f_{sweep-anode} = \frac{\dot{n}_{sweep}}{\dot{n}_{sweep} + \dot{n}_{O_2}}. \quad (6\text{-}11)$$

The current density and active cell area are then specified, yielding the total operating current. Care must be taken to insure that the specified inlet gas flow rates and total cell current are compatible. The minimum required inlet steam molar flow rate is the same as the steam consumption rate, given by:

$$\dot{N}_{i,H2O,\min} = \Delta\dot{N}_{H2O} = \frac{I}{2F} N_{cells} = \frac{i A_{cell}}{2F} N_{cells} = \Delta\dot{N}_{H2} \quad (6\text{-}`2)$$

which is of course also equal to the hydrogen production rate.

Once the total and per-cell hydrogen production rates are known, the outlet flow rates of hydrogen and steam on the cathode side and oxygen on the anode side can be determined. The flow rates of any inert gases, the anode-side sweep gas, and any excess steam or hydrogen are the same at the inlet and the outlet. Once all these flow rates are known, the summations in Eqn. (6-1) can be evaluated. The product summation must be evaluated initially at a guessed value of the product temperature, T_P in order to satisfy Eqn. (6-1). This algorithm can then be imbedded in a loop so that a full numerical "sweep" can be performed. We have implemented this procedure in Matlab. The Matlab model provides accurate estimates of electrolyzer operating voltage (and corresponding electrolyzer efficiency) and outlet temperatures, for any specified electrolyzer heat loss or gain, gas flow rates, current density, and per-cell *ASR(T)*. This electrolyzer model was developed for incorporation into system-level electrolysis plant models being developed using HYSYS [23] system simulation software. With a realistic electrolyzer model incorporated into the overall HYSYS plant model, good estimates of overall hydrogen-production efficiencies can be obtained over a wide range of prospective operating conditions.

VII. CONCLUSIONS

GAMMA code that is developed as part of ROK/US –I-NERI project has been verified using a number of experimental results. Results from GAMMA code agree very well with two bulb diffusion experimental results. Turbomachinery models that were developed separately using the Newton-Ralphson method to improve the convergence and to make more detailed calculations of the turbomachinery were verified well with GTHTR300 turbomachinery design basis with good agreements. The coupling scheme of VHTR and the high temperature steam electrolysis process to produce hydrogen using the nuclear energy has been proposed and some calculations of the electrolysis power requirements were made using Nernst equation. Overall, GAMMA code provides good results as compared with test data. We will implement the turbomachinary models and the hydrogen production model of the high temperature steam electrolysis into GAMMA code in the near future.

ACKNOWLEDGMENTS

This work was supported through the U.S. Department of Energy's Power Conversion Program and Nuclear Hydrogen Initiative Program under DOE Idaho Operations Office Contract DE-AC07-99ID13727.

REFERENCES

1. C. H. Oh, R. Barner, C. Davis, and S. Sherman, "Evaluation of Working Fluids in an Indirect Combined Cycle in a Very High Temperature Gas-Cooled Reactor," Nuclear Technology , Vol.156, No.1, 2006.

2. P.E. Macdonald et al., "The Next Generation Nuclear Plant- Insights gained from the INEEL Point Design Studies," INEEL, INEEL/CON-04-01563, 2004.

3. General Atomics, *Gas Turbine-Modular helium Reactor (GT-MHR) Conceptual Design Description Report*, 910720, Revision 1, July, 1996.

4. D.R. Nicholls, "Status of the Pebble Bed Modular Reactor," *Nuclear Energy* **39**, No.4, 2000.

5. C. H. Oh, C. Davis, L. Siefken, R. Moore, H. C. NO, J. Kim, G.C. Park, J.C. Lee, and W. R. Martin, "Development of Safety Analysis Codes and Experimental Validation for a Very High Temperature Gas-Cooled Reactor," Final Report, Idaho National Laboratory, INL/EXT-06-01362, March 2006.

6. T. Poinsot and D. Veynante , Theoretical and Numerical Combustion, R.T. Edwards Inc., 2001.

7. D. A. Nield. and A. Bejan A., Convection in Porous Media, Springer-Verlag, New York ,1999.

8. J. P. Holman, J. P., 1986, Heat Transfer, Sixth Edition, McGraw-Hill Book Company, New York.

9. J. O. Hirschfelder , C. F. Curtiss., and R. B. Bird , Molecular Theory of Gases and Liquids, John Wiley & Sons, New York ,1964.

10. W. M. Kayes, and M.E. Crawford, *Convective Heat and Mass Transfer, Second Edition*, McGraw-Hill Book Company, New York, 1980.

11. B. E. Poling, J. M. Prausnitz, and J. P. O'Connell,2001. The Properties of Gases and Liquids, Fifth ed., McGraw-Hill, New York.

12. K. Raznjevic, 1976. Handbook of Thermodynamic Tables and Charts, Hemisphere, Washington.

13. F. H. Harlow, F.H. and A. A. Amsden, 1971. A Numerical Fluid Dynamics Calculation Method for All Flow Speeds. J. Chem. Phys. 8, 197.

14. J. B. Duncan, J.B. and H. L. Toor, 1962. An experimental study of three component gas diffusion. A.I.Ch.E. Journal 8(1): 38-41.

15. J. H. Kim, H. M. Kim, H. C. NO, Assessment of HTGR Helium Compressor Analysis Tool based on Newton-Ralphosn Numerical Application to Throiughflow Analysis, ICONE14-89411, July 17-20, Miami, Florida, 2006.

16. N.A. Cumpsty, "Compressor Aerodynamics", Longman Scientific & Technical ,1989.

17. J.D. Denton, "Throughflow Calculation for Transonic Axial Flow Turbines," Journal of Engineering for Power, Transactions of the ASME, Vol. 100, pp. 212-218 ,1978.

18. T. Takizuka, S. Takata, X. Yan, S. Kosugiyama, S. Kantanishi and K. Kumitomi, "R&D on the Power Conversion System for Gas Turbine High Temperature Reactors," Nuclear Engineering and Design, North-Holland Publishing Company, pp.329-346, 2004.

19. Independent Technology Review Group, Design Features and Technology, Uncertainties for the Next Generation Nuclear Plant, INEEL/EXT-04-01816, 2004.

20. C. H. Oh, C.B. Davis, J. Han, R. Barner, S. Sherman, R. Vilim, Y. Lee, W. Lee, INEEL, 2006, HyPEP FY06 Report: Models and Method, INEEL/EXT-06-11725, September 2006.

21. I. Sochet, I., J. L. Rouyer, and P. Hemmerich, 2004, "Safe Hydrogen Generation by Nuclear HTR," Paper 4261, Proceedings of ICAPP '04, Pittsburgh, PA, USA, June 13-17.

22. C. S. Smith, S. Beck, and B. Galyean, 2005, An Engineering Analysis for Separation Requirements of a Hydrogen Production Plant and High-Temperature Nuclear Reactor, INL/EXT-05-00137 Rev 0, March 2005.

23. Aspen Technology, HYSYS Process Version 2.2.2, www.aspentech.com,